Available online at www.sciencedirect.com
SCIENCE DIRECT
Coordination Chemistry Reviews 250 (2006) 1737–1754
COORDINATION CHEMISTRY REVIEWS
www.elsevier.com/locate/ccr

Review

Hole-burning spectroscopy of coordination compounds

Hans Riesen *

School of Physical, Environmental and Mathematical Sciences, University College, The University of New South Wales, ADFA, Canberra ACT 2600, Australia

Received 14 November 2005; accepted 23 January 2006
Available online 22 March 2006

Contents

Abstract

Electronic transitions in condensed phases are subject to inhomogeneous broadening, caused by the variation of local fields. Even in extremely well defined crystals, this broadening is on the order of magnitude of 1 cm^{-1} (30 GHz), obscuring valuable information about the electronic structure. There are several laser-based techniques that can overcome the inhomogeneous broadening and the homogeneous (or natural) line width may be approached at low temperatures. This latter line width may be as narrow as 30 Hz (1×10^{-9} cm^{-1}) at liquid helium temperatures. In this article an overview of spectral hole-burning mechanisms and their application to coordination compounds is given, and recent progress in chromium(III) systems is emphasized. In the past, the main subject of investigations by spectral hole-burning has been the temperature dependence of the homogeneous line width and ultimate spectral resolution was sought. However, even at moderate resolutions of ca. 30 MHz (0.001 cm^{-1}),

* Tel.: +61 2 6268 8679; fax: +61 2 6268 8017.
E-mail address: h.riesen@adfa.edu.au.

doi:10.1016/j.ccr.2006.01.016

spectral hole-burning is a very powerful technique that is capable of unraveling *g*-factors in low magnetic fields, dynamics of water molecules of crystallization, spin-lattice relaxation rates and hyperfine (and super-hyperfine) interactions in the excited state and the ground state.

Besides being a highly successful spectroscopic technique, spectral hole-burning also has many potential applications in areas such as ultra-high density optical data storage (>100,000 GB/cm^3) and processing, laser frequency stabilization, portable frequency standards, etc. Coordination compounds may be tailored to fulfill the stringent requirements of such applications.

Keywords: Electronic transitions; Hole-burning; Hyperfine interaction; Homogeneous broadening; Inhomogeneous broadening; Coordination compounds; Zeeman effect

1. Introduction

Laser spectroscopy of condensed phases has advanced rapidly since the advent of tunable single frequency dye lasers in the early 1970s and, over the last three decades, energy-selective techniques, such as spectral hole-burning, have become invaluable and highly successful spectroscopic tools for the detailed investigation of electronic structures.

The discovery of transient and persistent spectral hole-burning in optical spectra of solids can be credited to Szabo [1], and Kharlamov et al. [2] and Gorokhovskii et al. [3], respectively. Szabo observed *transient* hole-burning in the R_1-line of ruby, whereas Kharlamov et al. and Gorokhovskii et al. reported *persistent* spectral hole burning in the $^1\pi$–π^* transition of perylene and 9-aminoacridine in frozen ethanol and the Q-band of free base phthalocyanine in an *n*-octane Shpol'skii matrix, respectively.

However, spectral hole-burning in optical spectra of *condensed* phases at modest resolutions was reported before these articles. For example, Soffer and McFarland reported some evidence for transient spectral hole-burning in an early paper (1966) entitled "Frequency locking and dye spectral hole-burning in Q-spoiled lasers" where they investigated some aspects of spectral hole-burning in phthalocyanine containing solutions [4]. In a related paper, Spaeth and Sooy reported in 1968 that cryptocyanine in methanol displays transient spectral hole-burning under laser irradiation (ruby laser at 694.3 nm) at room temperature and that the spectral width of the hole is less than 20 Å [5].

In the same year as the reports by Kharlamov et al. [2] and by Gorokhovskii et al. [3] were published, Hager and Willard delivered a paper entitled "Wavelength-selective bleaching (burning holes) in the optical spectra of solvated electrons in organic glasses" [6]; they reported the observation of spectral holes in infrared transitions of trapped electrons in frozen 3-methylpentane and methyltetrahydrofuran glasses at 25 K.

In the following we will present a short introduction to the concepts and properties of homogeneous and inhomogeneous line widths and the mechanisms of spectral hole-burning. Several excellent reviews of hole-burning spectroscopy in organic molecules and rare earth containing solids have been published previously. We note here that Macfarlane and his group at the IBM Almaden Research Center have made seminal contributions to this field in general, and its application to rare earth ions in solids in particular. His early review with Shelby can be considered as a major cornerstone in the development of laser spectroscopy of the solid state [7]. Other major contributors to this field include Moerner [8], Völker [9], Friedrich and Haarer [10], Wild et al. [11], Meltzer and co-workers [12], and Manson and co-workers [13]. The interested reader is referred to the many excellent contributions by these researchers.

However, with the exception of the highly interesting and original work by Strauss et al. on infrared hole-burning in vibrational excitations [14] and the investigations by the author of the present article on electronic transitions [15], the application of hole-burning spectroscopy to coordination compounds has received little attention despite its outstanding power.

1.1. The homogeneous line width and its temperature dependence

The simplest electronic model system consists of an electronic ground state and an electronically excited state. The width of the electronic origin, the transition between the zero point energy of the ground state and the zero point energy in the excited state, is governed by the lifetime of the excited state, T_1, and the pure dephasing time T_2^*. These two times are often combined in an effective dephasing time T_2, as shown in the following equation:

$$\frac{1}{T_2} = \frac{1}{2T_1} + \frac{1}{T_2^*} \tag{1}$$

Using the effective dephasing time the homogeneous line width of an electronic origin between the two electronic levels can be described by

$$\Gamma_{\text{hom}} = \frac{1}{\pi T_2}\sqrt{1 + \omega_1^2 T_1 T_2} \tag{2}$$

The second term in the square root describes the power broadening by the probing laser. In this term ω_1 denotes the Rabi frequency, which is proportional to the scalar product of the electric field vector of the radiation field and the transition dipole moment μ:

$$\omega_1 = \frac{\mu E}{\hbar} \tag{3}$$

The inverse of the Rabi frequency is a measure of the time needed for an ensemble to reach ≈50% excited state population.

The power term can be neglected if very low laser powers are used and the homogeneous line width is then approximately given by

$$\Gamma_{\text{hom}} \approx \frac{1}{\pi T_2} \tag{4}$$

Dephasing processes can be due to electron–phonon interactions or electron-spin–electron-spin and electron-spin–nuclear-spin

interactions. If the electronic ground state has no spin and orbital degeneracy (diamagnetic species), dephasing is based on the interactions of phonons (vibrations) with the electronic system and can be frozen out by cooling the sample to liquid helium temperatures. In this case, the lifetime limited homogeneous line width, as given in Eq. (5), is approached:

$$\Gamma_{\text{hom}} \approx \frac{1}{2\pi T_1} \tag{5}$$

Thus, optical line widths can, in principle, be as narrow as 30 Hz for spin and parity forbidden transitions with excited state lifetimes of approximately 5 ms and about 15 MHz for electric dipole allowed transitions with excited state lifetimes of about 10 ns.

In the case of paramagnetic centers, electron-spin–electron-spin and electron-spin–nuclear-spin interactions govern the dephasing time T_2^* at liquid helium temperatures. Dephasing processes based on electron-spin–electron-spin interactions can be minimized by working with extremely dilute samples and high external magnetic fields. In a very early paper, Bloembergen has estimated that these interactions become negligible if the average distance between paramagnetic centers is much larger than 100 Å [16]. Thus, to avoid electron-spin–electron-spin interactions, concentrations should be much lower than 4×10^{-4} mol/L. Electron-spin–nuclear-spin interactions cannot be avoided if the system contains atoms with nuclear spins. It is important to note here that in the case of the so-called super-hyperfine limit (only interactions between the electron spin of the guest with nuclear spins of the host are present) the line width is not defined anymore [17]. In this case the nuclear spins close to the paramagnetic centre are detuned from the spins of the bulk due to the large magnetic moment of the optical centre. As a consequence mutual spin–flips are subject to a distribution that displays a decrease of the rate with decreasing distance between the nuclear spin and the paramagnetic centre and only spins far from the paramagnetic centre will flip at early times. However, as time progresses nuclear spins close to the optical centre will also flip. Hence the dephasing rate increases with increasing time, resulting in an increase of the observed line width. The phenomenon of detuned nuclear spins in the nearest neighborhood of paramagnetic centres has been coined the "frozen core" effect [18–20] and the variation of the dephasing rate with time has been observed in photon-echo measurements on ruby, LaF_3:Er^{3+} and $YLiF_4$:Er^{3+} [17].

Both for paramagnetic (diluted to a reasonable level) and diamagnetic species, dephasing processes are, in general, dominated by electron–phonon (vibration) interactions at higher temperatures (>6 K).

Fig. 1 illustrates the dynamic broadening mechanisms that are based on the interaction between the electronic system and vibrations. These four mechanisms broaden optical transitions that involve either level *a* or *b* as the initial or the final state i.e. *a* and *b* can be excited state or ground state levels. The direct process (I) is important for coordination compounds due to the relatively high density of phonon states at low frequencies (i.e. a high number of accessible vibrational excitations). If the energy difference between the two electronic levels is larger than the maximum vibrational frequency a multi-phonon process may bridge the gap. This latter process is strongly dependent on the number of phonons that have to be created or annihilated and the relative displacement of the two states along the metal–ligand normal coordinate. The contribution by a direct one-phonon relaxation process between levels *a* and *b*, separated by ΔE, to the line width of a transition involving either level *a* or *b*, can be calculated by using Eqs. (6) and (7) for the absorption and emission of one phonon, respectively:

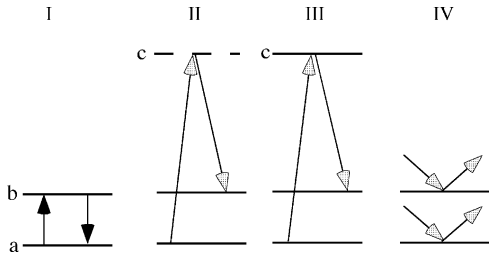

Fig. 1. Schematic representation of the direct (I), two-phonon Raman (II), Orbach (III) and intrinsic Raman scattering processes (IV). In II and III, c is a virtual and real state, respectively.

$$\Delta\Gamma_{\text{direct}}(a) = \frac{1}{2\pi T_1(b)}\bar{n}(\Delta E) \tag{6}$$

$$\Delta\Gamma_{\text{direct}}(b) = \frac{1}{2\pi T_1(b)}(\bar{n}(\Delta E) + 1) \tag{7}$$

where $\bar{n}(\Delta E) = 1/[\exp(\Delta E/k_B T) - 1]$, k_B the Boltzmann constant and $[T_1(b)]^{-1}$ is the relaxation rate $b \rightarrow a$ at 0 K. It is obvious that the 0 K contribution by the direct process has a finite value, $1/(2\pi T_1(b))$, for level *b* whereas it is zero for level *a*.

Fig. 2 illustrates the contribution by the direct process to the line width of an optical transition with final or initial level *a* or *b*. Consider, for example, the case where $k_B T/\Delta E = 1$. From Fig. 2 (dashed lines) it then follows that the contributions, $\Delta\Gamma_{\text{direct}}$

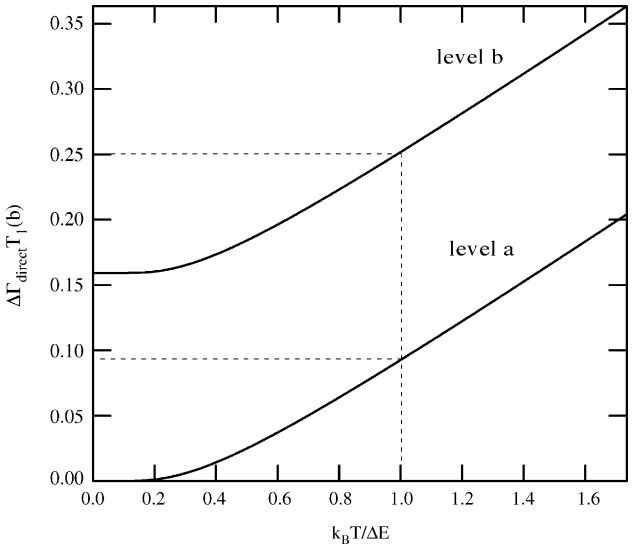

Fig. 2. Contributions by the direct one-phonon process to the line width of a transition that involves either level *a* or level *b*. ΔE is the energy difference between *a* and *b*; $1/T_1(b)$ is the direct one-phonon rate from $b \rightarrow a$ at $T = 0$ K.

to the line width of transitions involving level a or level b are $\approx 0.09/T_1(b)$ and $\approx 0.25/T_1(b)$, respectively. Thus, for a typical splitting of $\Delta E = 20\,\mathrm{cm}^{-1}$, a relatively low 0 K relaxation rate $1/T_1(b)$ of $1 \times 10^9\,\mathrm{s}^{-1}$ and a temperature $T = 29$ K contributions of 90 MHz ($0.003\,\mathrm{cm}^{-1}$) and 250 MHz ($0.008\,\mathrm{cm}^{-1}$) result for a and b, respectively. Often relaxation rates are in the picosecond or even femtosecond range and hence the line width contribution by the direct process can become very large (ca. 1–100 cm^{-1}). This rationalizes the fact that electronic origins to higher-lying excited states can be much broader in comparison with the electronic origin to the lowest-excited state.

The temperature dependence of electronic origins is often governed by two-phonon Raman processes (II). In the case of weak quadratic electron–phonon coupling, the contribution to the line width by this process can be described by Eq. (8) [21]:

$$\Delta\Gamma_{\mathrm{Raman}} \propto \int_0^{\infty} \rho(\omega)^2 \bar{n}(\omega)[\bar{n}(\omega) + 1]\,\mathrm{d}\omega \tag{8}$$

where $\rho(\omega)$ is the weighted density of phonon states. The Raman process will broaden transitions involving levels a or b by the same amount. (Fig. 1 shows only the two-phonon Raman process initiating from level a.) Applying the Debye approximation for the density of phonon states in Eq. (8), the famous "T^7" temperature dependence for the two-phonon Raman process results, as given in Eq. (9) [22], where T_{D} is the Debye temperature:

$$\Delta\Gamma_{\mathrm{Raman}} = \bar{\alpha}\left(\frac{T}{T_{\mathrm{D}}}\right)^7 \int_0^{T_{\mathrm{D}}/T} \frac{x^6\,\mathrm{e}^x}{(\mathrm{e}^x - 1)^2}\,\mathrm{d}x \tag{9}$$

Although $\bar{\alpha}$ can, in principle, be calculated, it is best treated as a parameter. Fig. 3 illustrates the temperature dependence of the contribution by a two-phonon Raman process to the line width. To render this figure generally applicable, $\Delta\Gamma_{\mathrm{Raman}}/\bar{\alpha}$ is plotted as a function of T/T_{D}. This graph shows that the T^7-dependence (dashed line) is followed at low temperatures only, being valid up to temperatures of $\approx 0.1 T_{\mathrm{D}}$. Fig. 3 highlights (dashed bars) an example with $T/T_{\mathrm{D}} \approx 0.3$ where a contribution of ca. $10^{-2}\bar{\alpha}$ is calculated. The parameter $\bar{\alpha}$ is of the order of magnitude of several hundred wave numbers. For example, the MgO:V^{2+} R-line displays a value of $\bar{\alpha} = 378\,\mathrm{cm}^{-1}$ and the Debye temperature is $T_{\mathrm{D}} = 760$ K for this material [23]; thus at $T = 228$ K the two-phonon Raman process leads to a broadening by $3.7\,\mathrm{cm}^{-1}$. We stress here that the parameter $\bar{\alpha}$ can be much larger for crystals of coordination compounds.

In coordination compounds, vibrations that couple to the electronic states are often best described as pseudo-local, because this class of compounds consists of discrete molecular units. If the angular frequency and lifetime of the pseudo-local modes in the ground electronic state are given by ω_0^i and τ_0^i, respectively, and their product $\tau_0^i\omega_0^i \gg 1$, Eq. (8) can be approximated by Eq. (10) [24–26] where a_i are coupling constants:

$$\Gamma_{\mathrm{Raman}} \approx \sum_i a_i \bar{n}(\omega_0^i)[\bar{n}(\omega_0^i) + 1] \tag{10}$$

Fig. 4 illustrates the contribution to the line width by the two-phonon Raman process of a local mode with angular frequency ω_0. Again, the graph is generally applicable. For example, if $k_{\mathrm{B}}T/\omega_0 = 1$ the contribution is approximately equal to the coupling constant a, which can be of the order of magnitude of tens of wave numbers. Thus a substantial line width increase results from an increase of the temperature when the system has low frequency vibrational modes that couple to the electronic state(s).

If the energy difference between levels a and b is much less than between a and c (where c is a real state) the Orbach process (III) broadens both a and b by equal amounts and the rate is proportional to $\bar{n}(\Delta E) = 1/[\exp(\Delta E/k_{\mathrm{B}}T) - 1]$ where ΔE is

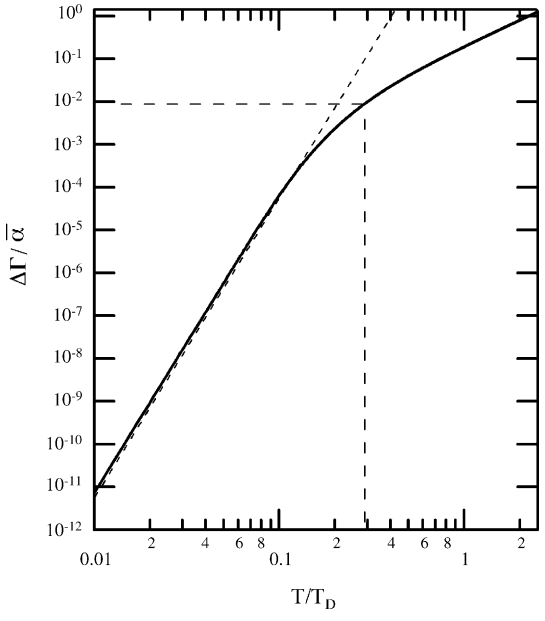

Fig. 3. Line width contribution (solid line) by the two-phonon Raman process as a function of temperature. The dashed straight line (that follows the solid line at low temperatures) indicates the "T^7" behavior.

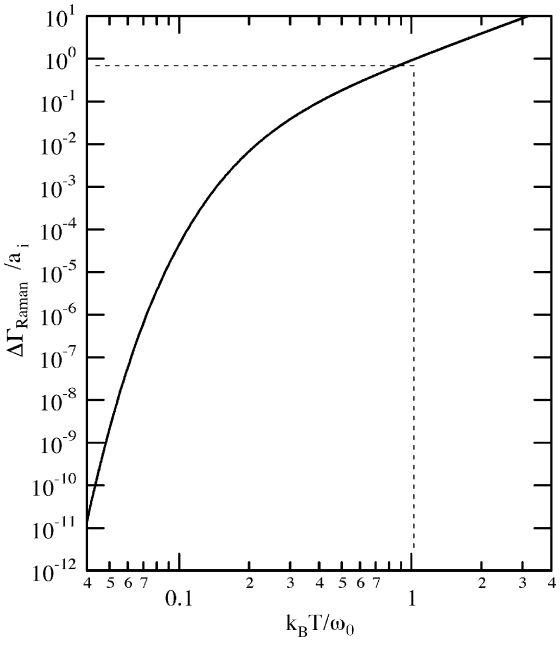

Fig. 4. Contribution by a local mode i (with coupling constant a_i) to the line width by the two-phonon Raman process as a function of temperature.

the energy difference between (a,b) and c. At low temperatures $\Delta E \gg k_B T$ and thus $\bar{n}(\Delta E) \approx \exp(-\Delta E/k_B T)$.

In addition to these three mechanisms, intrinsic Raman scattering (IV) may occur: this is a pseudo-elastic scattering process that dephases the total vibronic wave function. This process has the same functional dependence on temperature as the two-phonon Raman scattering discussed above.

1.2. Inhomogeneous broadening

Unfortunately, the homogeneous line width cannot be observed in conventional absorption and luminescence spectroscopy at low temperatures because all condensed phases suffer from the phenomenon of inhomogeneous broadening: the frequency of an electronic transition is subject to a distribution because each optical centre may have a (slightly) different environment. This is obvious for an amorphous system where there is no long range order and the chromophores are in disordered environments, leading to a massive inhomogeneous width. In the case of crystals, defects, unintentional impurities, strain, isotope distributions etc cause a variation of the local fields. For example, a slight variation of the metal–ligand distance R in coordination compounds leads to a significant change in ligand-field strength since the latter is proportional to $1/R^5$. Nevertheless, in very well defined crystalline systems the inhomogeneous width can be relatively low ($\approx$1 cm^{-1}).

Because electronic energies usually depend on many parameters, the resulting inhomogeneously broadened line shape is often Gaussian, in accord with the central limit theorem (see Fig. 5). Naturally, the inhomogeneous broadening strongly depends on the nature of the transition. For example, a charge transfer transition (e.g. metal-to-ligand charge transfer) is much more susceptible to variations in the local environment than, for example, a simple spin–flip transition, because the resulting electric dipole moment will strongly interact with local electric charges and dipoles. As a consequence, in an amorphous host, it can be expected that MLCT energies are substantially different for individual ligands in a complex such as $[Ru(bpy)_3]^{2+}$. It appears that this effect has been underestimated in the past. For spin–flip transitions within the same electronic configuration, ligand-field transitions, and charge-transfer excitations we can expect a range of the inhomogeneous broadening of electronic origins of about 1–100, 10–100 and 10–1000 cm^{-1}, respectively, with the lower and upper limits applicable to well defined crystals and highly disordered amorphous systems, respectively.

1.3. Spectral hole-burning mechanisms

Inhomogeneous broadening can be overcome by several laser techniques, including fluorescence line narrowing, spectral hole-burning and photon-echo experiments. In spectral hole-burning a subset of chromophores gets depleted in the ground state upon selective laser excitation, leading to a dip in the absorption, transmission or excitation spectrum. Spectral hole-burning is basically a sequential two photon process: the first photon is used to burn the center and the second photon is used in the readout of the spectral hole.

There are three mechanisms for spectral hole-burning. First, in photochemical hole-burning a subset of chromophores, within the inhomogeneously broadened transition, may undergo some chemistry in the excited state upon selective excitation. Characteristically, the photoproduct leads to new absorption features outside the inhomogeneous distribution. Specific mechanisms that lead to photochemical hole-burning include photoredox reactions, tautomerization, ligand exchange, conformer interconversion, etc. Fig. 6 schematically depicts an absorption spectrum before and after photochemical hole-burning has occurred at the laser frequency.

Second, non-photochemical hole-burning is a ubiquitous phenomenon in amorphous hosts but can also occur in crystalline systems such as inorganic hydrates. Upon the selective excitation of a subset of chromophores within the inhomogeneous distribution, host–guest interactions may be rearranged. These rearrangements may include hydrogen bonds, translational movements or rotations of chemical groups or the entire chromophore or host molecules. Characteristically, the rearranged host–guest subset leads to absorption features within the inhomogeneous distribution and, indeed, even close to the laser frequency. This is schematically depicted in Fig. 7.

Non-photochemical spectral hole-burning has often been interpreted by the so-called two-level systems (TLS) model [27], originally developed to rationalize the thermal properties of glasses at low temperatures [28]. The potential energy along any coordinate Q within an amorphous host will display a non-periodic behavior, as is schematically illustrated in Fig. 8. The TLS model then approximates this potential energy function as

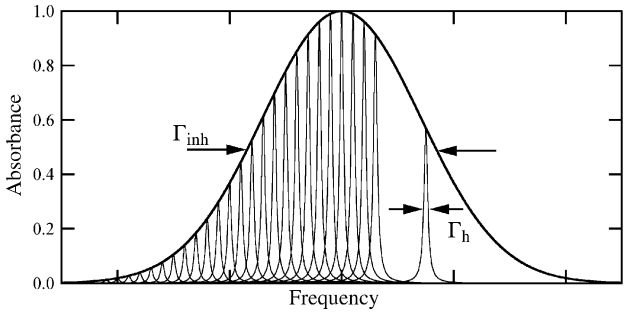

Fig. 5. Inhomogeneous broadening in condensed phases is caused by the distribution of transition frequencies due to the variation of local fields. Γ_{inh} and Γ_h denote the inhomogeneous and homogeneous line widths, respectively.

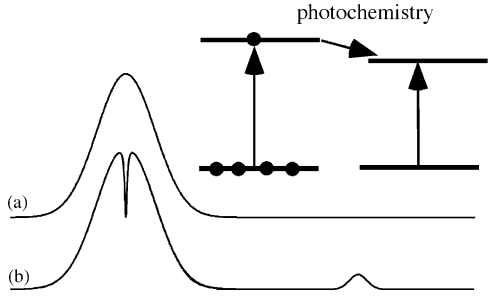

Fig. 6. Schematic representation of photochemical hole-burning. A selectively excited subset of chromophores undergoes chemistry in the excited state, resulting in ground state depletion at the laser frequency.

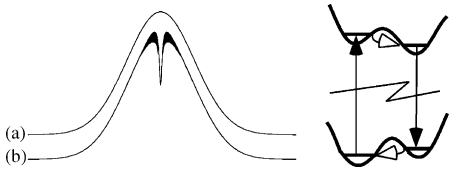

Fig. 7. Schematic representation of non-photochemical hole-burning. The absorption spectrum is shown before (a) and after (b) hole-burning. A simple TLS model that can rationalize non-photochemical hole burning is shown on the right.

a distribution of double well potentials. Because of the central limit theorem, it can be assumed that this distribution is close to Gaussian. A selectively excited subset of chromophores may tunnel to the adjacent well. After deactivation, the tunneling to the original ground state well may be very slow, resulting in long-lived holes. Naturally, both the tunneling in the excited state and the ground state will be subject to the distribution of double wells involved.

It has been argued that for the interpretation of non-photochemical hole-burning properties of impurities in amorphous systems two sets of TLSs have to be considered, namely the extrinsic and intrinsic TLSs which are due to the interaction between the guest with nearest and distant host neighbors, respectively [27,29].

Third, transient spectral hole-burning is, in principle, a universal phenomenon. Upon the selective excitation of a subset of chromophores a depletion of the ground state occurs at the laser frequency. This depletion lasts as long as the system takes to relax back to the initial ground state level. Thus it is obvious that it is much easier to perform experiments on long-lived excited states. Transient spectral hole-burning can be classified into three types, as is depicted in Fig. 9. Type I consists of a ground state

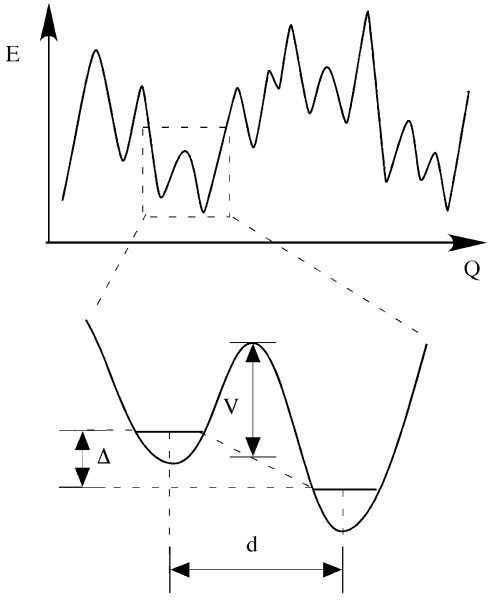

Fig. 8. Potential energy in an amorphous system. In the upper panel the potential energy along a coordinate Q in an amorphous host is shown. The lower graph shows one TLS (double well) with a definition of the parameters used to calculate the tunneling parameter λ.

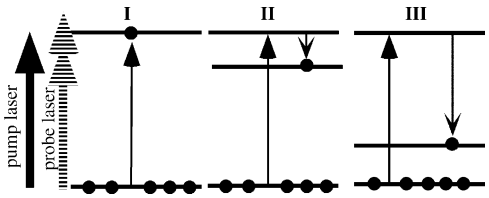

Fig. 9. Schematic representation of the three types of transient spectral hole-burning.

level and an excited state level and hence the readout has to be performed within the lifetime of the excited state; type II has a lower-lying metastable excited state that can act as a bottleneck if the latter has a long lifetime; type III has more than one ground state level due to electronic fine structure (ground state splitting caused by spin-orbit coupling and lower symmetry ligand fields), hyperfine interactions (electron-spin–nuclear-spin interaction within chromophore) and superhyperfine interactions (interactions of electron spin of chromophore with nuclear spins of host) or Zeeman levels in an external magnetic field.

1.4. Hole-burning kinetics

1.4.1. Hole growth

For an optically thin sample, in the absence of hole-filling and dispersion of hole-burning rates, and with the assumptions of a Lorentzian homogeneous line shape and that the laser line width is much narrower than the homogeneous line width, the normalized contour of a spectral hole, burnt at w_0, is given by following convolution [30,31]:

$$H(w - w_0, t) = \int_{-\infty}^{+\infty} \left[1 - \exp\left(-\frac{ktL(w' - w_0)\pi\Gamma}{2}\right)\right] L(w' - w)\,\mathrm{d}w' \tag{11}$$

where k is the hole-burning rate which is determined by the peak absorption cross section σ, the photon flux P and the quantum efficiency ϕ, $k = \sigma P\phi$. In Eq. (11), t is the time and Γ the full width at half maximum (FWHM) of a normalized Lorentzian line shape as given by

$$L(x - x') = \frac{1}{2\pi}\frac{\Gamma}{(x - x')^2 + (\Gamma/2)^2} \tag{12}$$

Figs. 10 and 11 show the evolution and width of a spectral hole as a function of kt. As time progresses the effective hole width grows dramatically, and, eventually, the hole shape becomes severely non-Lorentzian. A 35% depth results in a ca. 50% increase of the hole width. Ideally, very shallow holes are burnt in investigations where resolution is important, e.g. in experiments on Zeeman splittings in low magnetic fields. Extrapolation to zero time (burn fluence) yields a hole width that is equal to twice the homogeneous line width. From Figs. 10 and 11 it clearly follows that homogeneous line widths *have to be* estimated from extrapolation to zero fluence.

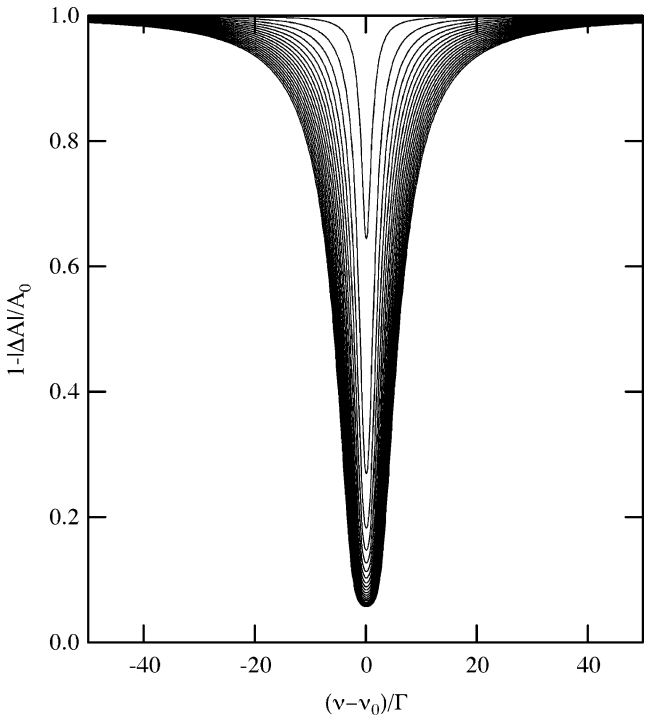

Fig. 10. Evolution of a spectral hole with time. The hole spectrum has been calculated using Eq. (11) with $kt = 5, 10, 15, \ldots, 95$.

The fractional hole depth, $|\Delta A|/A_0$, can be obtained [31] by integrating Eq. (11) at $w = w_0$:

$$\frac{|\Delta A(w_0,t)|}{A_0} = \int_{-\infty}^{+\infty}\left[1-\exp\left(-\frac{ktL(w'-w_0)\pi\Gamma}{2}\right)\right]L(w'-w_0)\,\mathrm{d}w' = 1-\exp\left(-\frac{kt}{2}\right)I_0\left(\frac{kt}{2}\right) \quad (13)$$

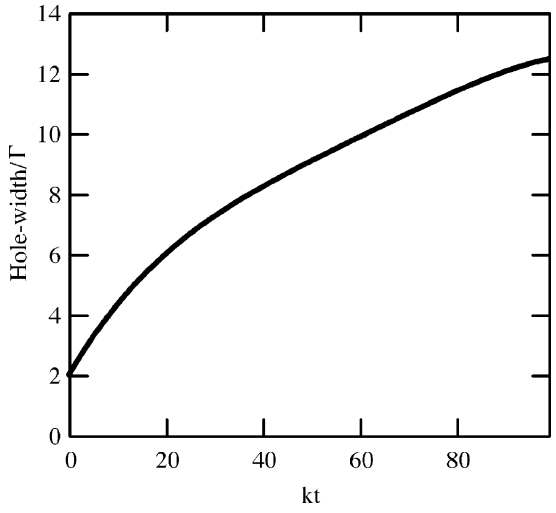

Fig. 11. Hole width in units of the homogeneous line width Γ, as a function of kt.

where I_0 is the modified Bessel function of zeroth order. The resulting hole growth kinetics as a function of kt is displayed in Fig. 12.

It is important to note here that the kinetics is not described by a simple exponential law but displays an *intrinsic* dispersion due to the fact that the Lorentzian has infinite wings. In other words, as the hole becomes deeper, the absorbance at the laser frequency due to the Lorentzian wing of transitions of near-resonant subsets of chromophores becomes important. Crystalline systems show relatively little disorder and thus the quantum efficiency for hole-burning is often well defined, so that Eq. (13) can indeed be applied. However, amorphous systems show a variation of hole-burning rates and this dispersion has to be taken into account. If the rate k is subject to a distribution function $P(k)$, the fractional hole depth is given by [31]:

$$\frac{|\Delta A(w_0,t)|}{A_0} = 1-\int_0^{+\infty} P(k)\exp\left(-\frac{kt}{2}\right)I_0\left(\frac{kt}{2}\right)\mathrm{d}k \quad (14)$$

In Ref. [32] the quantum efficiency was parameterized by $\phi = \exp(-a)$ and it was assumed that a is subject to a Gaussian distribution. Moreover, the random orientation of the absorbing center in an amorphous solid was taken into account. In this latter point, it is assumed that the molecular transition moment occurs along one axis only. Applying Eq. (14), the following integral equation then results

$$\frac{|\Delta A(w_0,t)|}{A_0} = D-\frac{3D}{2\Gamma_a}\sqrt{\frac{4\ln(2)}{\pi}}\int_0^{\infty}\int_0^{\pi}\times\exp\left(-\frac{P\exp(-a)\sigma\cos^2\theta}{2}t\right)\times I_0\left(\frac{P\exp(-a)\sigma\cos^2\theta}{2}\right)\cos^2\theta\sin\theta\,\mathrm{d}\theta\times\exp\left(-4\ln(2)\frac{(a-a_0)^2}{w^2}\right)\mathrm{d}a \quad (15)$$

where a_0 and Γ_a are the center and width of the distribution of a, respectively, and D is a parameter that takes into account that a fraction of centres cannot be burned a priori. We note here that the average quantum yield can then be calculated as $\langle\phi\rangle = \exp(-a_0)\exp(\Gamma_a^2/4)$.

The formalism of Ref. [32] is very much related to the previous work by Jankowiak et al. [33]. In this early work it was suggested that the tunneling parameter λ, as given by Eq. (16), is, most likely, subject to a Gaussian distribution:

$$\lambda = \frac{d\sqrt{2mV}}{\hbar} \quad (16)$$

In Eq. (16) d is the distance between the two wells along the normal coordinate, m the mass of the particle and V is the barrier height (see Fig. 8). The parameter λ determines the tunneling interaction, Δ, between wells according to

$$\Delta = \hbar\omega_0\,\mathrm{e}^{-\lambda} \quad (17)$$

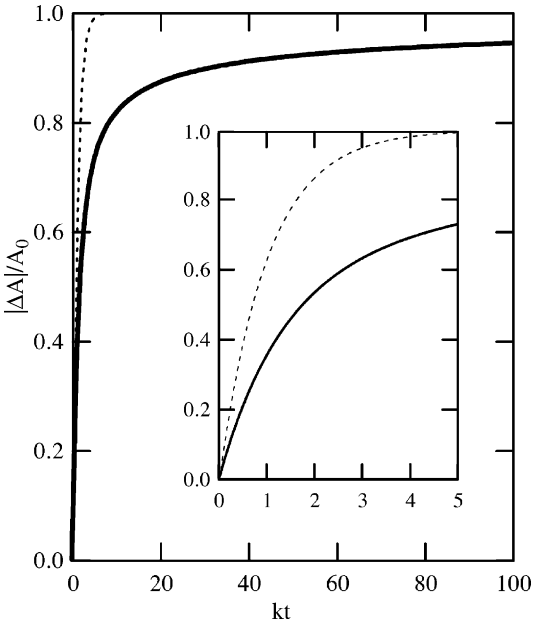

Fig. 12. Fractional hole depth, $|\Delta A|/A_0$, as a function of kt. The dashed line shows a simple exponential behavior. The solid line has been calculated by using Eq. (13).

where $\hbar\omega_0$ is on the order of magnitude of one quantum of a harmonic oscillator. The relaxation rate R, based on phonon-assisted tunneling, in a double well potential is proportional to Δ^2:

$$R = \Omega_0 \exp(-2\lambda) \tag{18}$$

where Ω_0 is an attempt frequency. Assuming an exponential function for the hole-growth, the following expression then results for the fractional hole depth if all sites can be bleached:

$$\frac{|\Delta A(t)|}{A_0} = \left(1 - \frac{1}{\sqrt{2\pi}} \int_{-\infty}^{+\infty} \exp\left(-\frac{x^2}{2}\right) \exp(-\Sigma_0 \xi(x) t)\, \mathrm{d}x\right) \tag{19}$$

with $x = (\lambda - \lambda_0)/\sigma_\lambda$, $\Sigma_0 = P\sigma\Omega_0\tau$ and $\xi(x) = \exp[-2(\lambda_0 + \sigma_\lambda x)]$ where P is the photon flux, σ is the peak absorption cross section of the homogeneous line, τ the excited state lifetime and σ_λ the standard deviation of λ. We note here that this latter equation neglects the intrinsic dispersion as is described by Eq. (14). However, in amorphous systems the dispersion of rates due to the variation of the tunneling parameter λ may be by far the most dominant effect, and hence Eqs. (15) and (19) yield comparable results. The expectation value for the hole-burning quantum efficiency is then given by $\langle\phi\rangle = \langle R\rangle/(\langle R\rangle + 1/\tau)$ with $\langle R\rangle = \Omega_0 \exp(-2\lambda_0) \exp(2\sigma_\lambda^2)$.

In a simpler approach, (a lower limit for) the initial quantum efficiency for spectral hole-burning can also be estimated by using the following equation:

$$\phi_i = \frac{lN_\mathrm{A}c(\Gamma_\mathrm{h})\left(\frac{\partial A}{\partial t}\right)_{t=0}}{A_0 \frac{1}{h\nu}(1 - 10^{-A_0})} = \frac{lN_\mathrm{A}c(\Gamma_\mathrm{h})h\nu\left(\frac{\partial A}{\partial F}\right)_{t=0}}{A_0(1 - 10^{-A_0})} \tag{20}$$

where N_A is Avogadro's number, $c(\Gamma_\mathrm{h})$ the concentration of chromophores within one homogeneous line width, Γ_h, in units of (mol/cm^3), l the optical path length in (cm), I the laser irradiance in (W/cm^2), F the fluence in (J/cm^2) and A_0 is the initial absorbance (optical density) at the laser frequency ν. Eq. (20) underestimates the hole-burning efficiency by a factor of 2–6 because it is based, again, on the assumption that the hole-growth is given by a simple exponential function. However, Eq. (20) can be applied to optically thick samples.

1.4.2. Spontaneous hole-filling

Non-photochemical spectral holes in amorphous systems are subject to spontaneous hole-filling due to tunneling in the ground state TLSs. Hence, after a while (typically 1 h) the initial hole area may be significantly reduced. If the hole-burning process involves the *translational* tunneling of a proton in the double well potential of a hydrogen bond, a decrease of the tunneling rate is expected upon deuteration because the mass m increases by a factor of 2. This isotope effect has been observed in hole-burning efficiencies (tunneling in the excited state) and spontaneous hole-filling (tunneling in the ground state).

Assuming a Gaussian probability density function for the rate-controlling tunneling parameter λ, Jankowiak et al. have shown [27,33] that the hole decay can be modeled by the following (dispersive first order kinetics) function:

$$\frac{|\Delta A(t)|}{A_0} = \left(1 - \frac{1}{\sqrt{2\pi}} \int_{-\infty}^{+\infty} \exp\left(-\frac{x^2}{2}\right) \exp(-\Omega_0 \xi(x) t)\, \mathrm{d}x\right) \tag{21}$$

This equation is related to Eq. (19) with the same meanings of the parameters but for a spontaneous process.

1.4.3. Spectral diffusion

As time progresses one often observes a broadening of the initial hole width in spectral hole-burning experiments. This so-called spectral diffusion is particularly pronounced in amorphous hosts but has also been observed in crystalline systems. Spectral diffusion is caused by rearrangements in the host; that is to say, mostly due to rearrangements within the intrinsic TLSs. These rearrangements may be due to slight structural changes or due to nuclear and/or electronic spin fluctuations. Spin fluctuations are usually relatively fast, so that in most experiments to date, they were not resolved in time, leading to an *effective* homogeneous line width. In contrast, structural changes occur on a much slower time scale and spectral diffusion caused by such variations is easily observed. Structural rearrangements certainly occur in amorphous hosts even at liquid helium temperatures because they are non-equilibrium systems. Since the surroundings are subject to variations, the transition frequency will also change and hence the spectral hole will broaden with time.

For amorphous systems, Fayer et al. [34] derived Eq. (22) for the contribution of spectral diffusion to the optical line width

$$\Gamma_\mathrm{SD} \propto \int_0^\infty P(R)[1 - \exp(-Rt_\mathrm{w})]\, \mathrm{d}R \tag{22}$$

where $P(R)$ is the probability density function for the relaxation rate R and t_w is the waiting time after the hole-burning event.

Again, it is plausible to assume a Gaussian distribution of the tunneling parameter λ, yielding following distribution function for the relaxation rate R where R_0 and σ are the average and standard deviation of R, respectively:

$$P(R)\,\mathrm{d}R = \frac{1}{\sigma\sqrt{2\pi}}\exp\left[-\frac{\{\ln(R/R_0)\}^2}{2\sigma^2}\right]\mathrm{d}(\ln R) \quad (23)$$

1.5. Correlation of energy levels

Many spectroscopic models assume full correlation between the energy levels of a particular chromophore; that is to say, energy differences between levels are thought to be constant within the inhomogeneous distribution. Full correlation has been denoted as the "rigid shift approximation" and has been, for example, extensively used in the modeling of magnetic circular dichroism (MCD) [35]. However, it turns out that the rigid shift approximation is often severely in error and energy levels are poorly correlated. This is certainly true for frozen glasses but may also be true in crystalline systems for transitions that are strongly dependent on the local surroundings (e.g. charge-transfer transitions).

1.6. Homogeneous line widths of higher-energy transitions

In general, transition metal complexes relax rapidly to the lowest-excited state upon excitation into a higher lying excited state. This relaxation is typically below the nanosecond timescale although some specific systems may display relatively slow relaxations within sublevels of the lowest-excited multiplet (e.g. thermalization within the $^3\pi^*$ state of a ligand-centered transition). Transient hole-burning is then of type II, as defined in Fig. 9, and, since the lifetime is usually much shorter than the pure dephasing time, the hole width is directly proportional to the lifetime of the higher-lying excited state and given by Eq. (5).

1.7. Potential applications of spectral hole-burning

Besides being a highly powerful tool for probing fine details of the electronic structures of molecules and ions, spectral hole-burning has also many potential applications in laser stabilization schemes (both with persistent and transient holes) [36,37], portable frequency standards [38], pulse shapers and filters [39], all-optical spectrum analyzer [40], quantum computing [41], etc. However, the prevailing driving force for hole-burning studies is the field of frequency [42] and/or time domain [43] optical storage (FDOS/TDOS). FDOS and TDOS schemes allow storage densities of >100 TB/cm^3 (1000 GB = 1 TB) at liquid helium temperatures [44]. To find a material with a large figure-of-merit, $\Gamma_{\mathrm{inh}}/\Gamma_{\mathrm{hom}}$, at room temperature remains the difficult challenge and is not unlike the quest for high temperature superconductors of the 1970s and 1980s.

For example, in the basic FDOS scheme, binary numbers are encoded in terms of the presence (1) and absence (0) of holes on a frequency grid. In comparison with current CD-R/RW and DVD-R/RW technology, the frequency domain adds an extra dimension to the effective data storage density.

2. Experiment

2.1. Persistent spectral hole-burning

Persistent spectral holes can be burnt and read out in excitation or absorption. After keeping the laser at constant wavelength for a certain period of time, it is scanned across the inhomogeneous profile to reveal the dip in the absorption/excitation spectrum. This is the simplest experiment because the hole-burning and readout process can be undertaken on a slow timescale.

2.2. Transient spectral hole-burning

There are basically two experiments that can be employed to conduct transient spectral hole-burning. In the first case a pump and a probe laser are used and the measurement is performed under steady-state conditions. In the second case the experiment uses only one laser: after a short burn period at constant wavelength, the laser frequency is slewed across the absorption profile to reveal the spectral hole. Laser diodes are highly suitable for this experiment since their frequency can be slewed over 30 GHz on the nanosecond–microsecond time scale by changing the injection current. Naturally, if the laser frequency is scanned too rapidly the laser line width will broaden according to the Fourier transform limit (Eq. (5)). Fig. 13 illustrates a typical transient hole-burning measurement, employing a diode laser and Fig. 14 shows a basic experimental set-up. We note here that, in general, in *excitation* transient holes cannot be burnt and read out with a single laser.

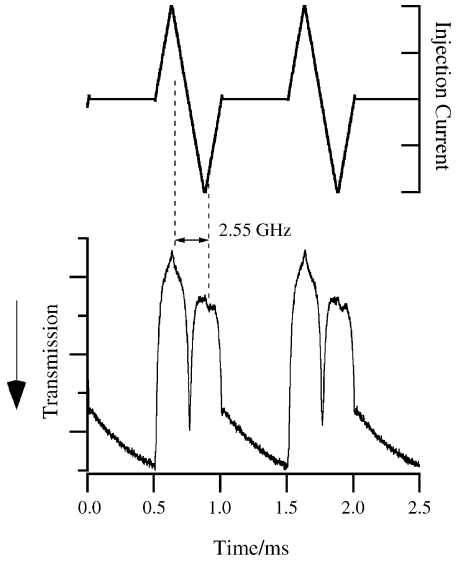

Fig. 13. Transient spectral hole-burning with one diode laser. The injection current, and thus the laser frequency, is kept constant for the burn period and then ramped for the readout. The transmission of the transmitted laser beam is monitored, revealing the spectral hole.

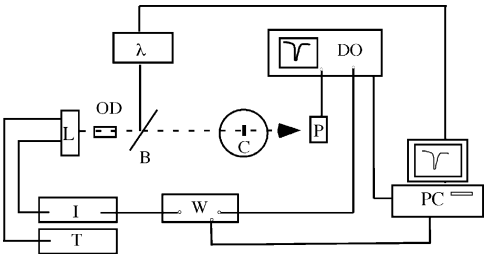

Fig. 14. Basic set-up for transient hole-burning spectroscopy with a diode laser (L). Optical feedback to the laser is avoided by an optical diode (Faraday isolator, OD). The laser is current (I) and temperature (T) controlled and the wavelength is measured by a wavemeter (λ). The injection current (I) is modulated by a wavefunction generator (W) and the signal, measured by a photodiode (P) is averaged on a digital oscilloscope (DO) and subsequently on a computer (PC). The sample is kept in a variable-temperature cryostat (C).

3. Spectral hole-burning of coordination complexes in amorphous systems

3.1. Spectral holes in the R-lines ($^2E \leftarrow {}^4A_2$) of chromium(III) complexes in amorphous hosts

In some early work, non-photochemical persistent spectral holes in the R_1-line (lower-energy $^2E \leftarrow {}^4A_2$ transition) of $[Cr(en)_3]^{3+}$ embedded in ethylene glycol-H_2O (2:1, v/v) glass and poly(vinyl alcohol) were investigated [45]. Hole widths on the order of magnitude of 300 MHz (1/100 cm^{-1}) were observed at 1.8 K, indicating an upper limit for the effective homogeneous line width of 150 MHz. We note here that these line widths were limited by electron-spin–electron-spin interactions due to the relatively high concentrations of $[Cr(en)_3]^{3+}$ (0.01 and 0.02 M for the ethylene glycol–H_2O glass and the poly(vinyl alcohol), respectively) and spectral diffusion within the amorphous hosts. It was found that holes are subject to spontaneous hole-filling and decay to about 50% of their initial area within 1 h. Equations, based on a constant and Gaussian distribution for the tunneling parameter λ, were applied to the data of spontaneous hole-filling, but the experimental accuracy was not adequate to discriminate between the two models. Importantly, it was found that the two ^2E levels are poorly correlated leading to very broad side holes for the R_2-line. Also, from the absence of side holes within 30 GHz it was concluded that the ±3/2 and ±1/2 Kramers doublets of the $^4A_2$ are also poorly correlated.

In some related work, the correlation of the zero field splittings of the $^4A_2$ and ^2E multiplets were systematically investigated for the $[Cr(bpy)_3]^{3+}$ complex in a variety of amorphous hosts [46]. Fig. 15 shows 1.5 K hole-burning results for the R_1-line in four different amorphous hosts. The observation of the side hole at approximately 30 GHz is due to the $^4A_2$ ground state splitting. The width of this side hole, in comparison with the resonant hole at the laser frequency, is a direct measure of the correlation of the ±3/2 and ±1/2 Kramer's doublets of the

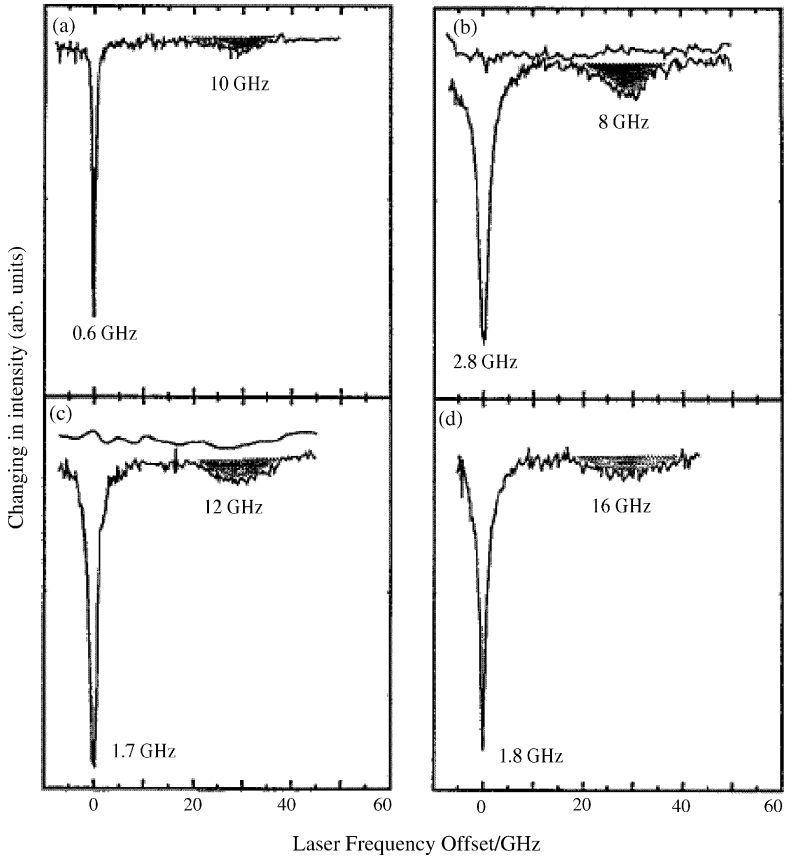

Fig. 15. Non-photochemical spectral hole-burning at 1.5 K in the R-lines of $[Cr(bpy)_3]^{3+}$ in (a) glycerol, (b) ethanol/methanol (4:1, v/v), (c) nafion and (d) sol–gel derived SiO_2. The hole widths are given for the resonant hole and the side hole. Holes were burnt to 25–30% depth at ca. 729.5 nm. Adapted from Ref. [46].

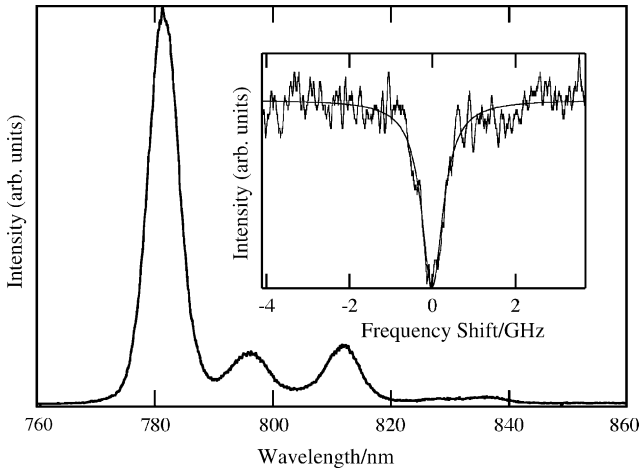

Fig. 16. Non-selectively excited (Ar^+ laser 488 nm) luminescence spectrum of $[Cr(NCS)_6]^{3-}$ in glycerol at 2.5 K. The insert shows a typical spectrum for a non-photochemical spectral hole burnt into the R_1-line at 780.49 nm. A Lorentzian line shape is fitted to the hole [48].

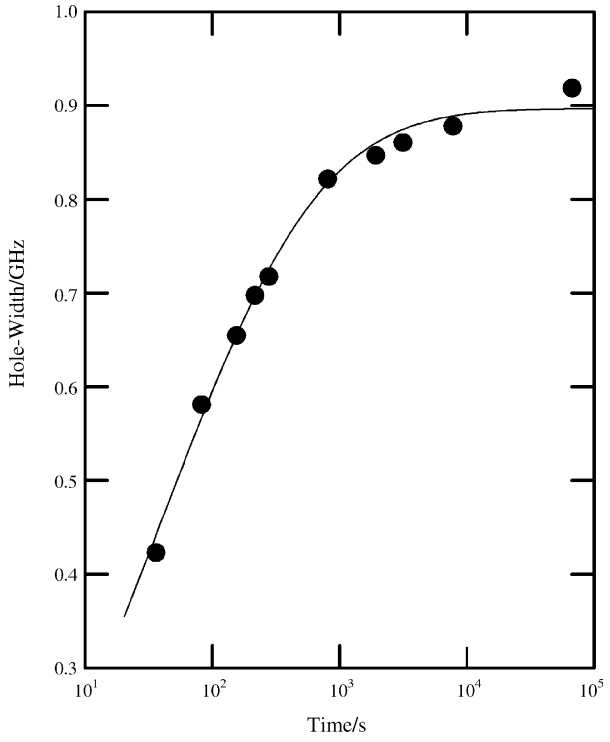

Fig. 17. Width of a spectral hole in the R_1-line of $[Cr(NCS)_6]^{3-}$/glycerol at 2.5 K as a function of waiting time, t_w. The solid line is a fit to the integral Eq. (22), using Eq. (23) for the distribution of R, with $\sigma_\lambda = 1.99$ and $R_0 = 0.016\,s^{-1}$ [48].

ground state. This width ranges from 8 GHz in ethanol/methanol glass (4:1, v/v) to 16 GHz in a sol–gel derived SiO_2 glass, indicating, indeed, a poor correlation of the levels, and thus a failure of the rigid shift approximation. The variations of the zero field splittings in the ^2E excited state and the $^4A_2$ ground state were analyzed in terms of low symmetry perturbations of the nominally trigonal complex. From these investigations it followed that data obtained by optically detected magnetic resonance and EPR in amorphous systems have to be interpreted with caution.

The low symmetry fields were also probed by investigating the effect of an external magnetic field on a hole burnt into the R_1-line (lower energy $^2E \leftarrow {}^4A_2$ transition) of $[Cr(bpy)_3]^{3+}$ in glycerol [47]. The fact that electronic structures of complexes are subject to distributions of lower symmetry fields in amorphous hosts, and hence energy levels are poorly correlated, is the most significant caveat of these investigations.

Spectral diffusion was investigated for the R_1-line of $[Cr(NCS)_6]^{3-}$ in glycerol [48]. Magnetic field effects in hole-burning of the R_1-lines in this system were previously used to demonstrate the feasibility of a hole readout scheme based on sweeping the magnetic field whilst keeping the laser frequency constant ("Zeeman scanning") [49]. $[Cr(NCS)_6]^{3-}$ is a system that exhibits a pronounced nephelauxetic effect, resulting in a very low energy of the ^2E multiplet (see Fig. 16).

In the range of 10 to 10^5 s, the time dependence of the spectral hole width displays a non-logarithmic behavior which can be described by using a Gaussian distribution for the tunnel parameter λ of the TLSs with $\lambda_0 = 15.9$ and $\sigma \approx 2$ (Fig. 17). This investigation established that spectral diffusion is a major factor for hole widths of electronic transitions in coordination compounds embedded in amorphous systems. Thus the potential of hole-burning experiments for determining subtle details of the electronic structure of coordination compounds *in amorphous hosts* is somewhat limited, and faster experiments, such as photon-echo measurements, are required. By comparison of the data with $[Cr(oxalate)_3]^{3-}$/glycerol it was concluded that the nephelauxetic effect does not enhance spectral diffusion in the title system. Importantly, from this work it also followed that spectral diffusion parameters in organic glasses of the $^2E \leftarrow {}^4A_2$ spin–flip transition and $^1\pi$–π^* transitions of organic molecules are comparable. These two findings indicate that spectral diffusion in amorphous systems is largely governed by host properties.

The temperature dependence of the effective homogeneous line width was also reported. The data shown in Fig. 18 indicates that the direct process to the R_2 level, and two-phonon Raman processes, govern the line width above >10 K. Interestingly, these two processes appear to yield a significant deviation from a simple $T^{1.3}$ law. This is in contrast to previous investigations of organic systems that were shown to follow, almost universally, a $T^{1.3}$ temperature dependence of the hole width [50].

In some recent work the effects of host deuteration on the spectral hole-burning efficiency (see Fig. 19) and spontaneous hole-filling of $[Cr(oxalate)_3]^{3-}$ in ethylene glycol/water (2:1, v/v) were investigated [51]. In line with previous findings in organic systems [52], the (initial) hole-burning efficiency is reduced by a factor of ca. 15 upon full deuteration of the glass. This reduction can be rationalized by a simple two level system model where tunneling of hydrogen atoms between the two wells of a double well potential occurs. Deuterium is heavier by a factor of 2 and hence the tunneling rate is slowed down. This work corroborates the significance of a 1000-fold *increase* of the hole-burning efficiency upon partial deuteration in $NaMgAl(oxalate)_3{\cdot}9H_2O$:Cr(III) (see below) [53].

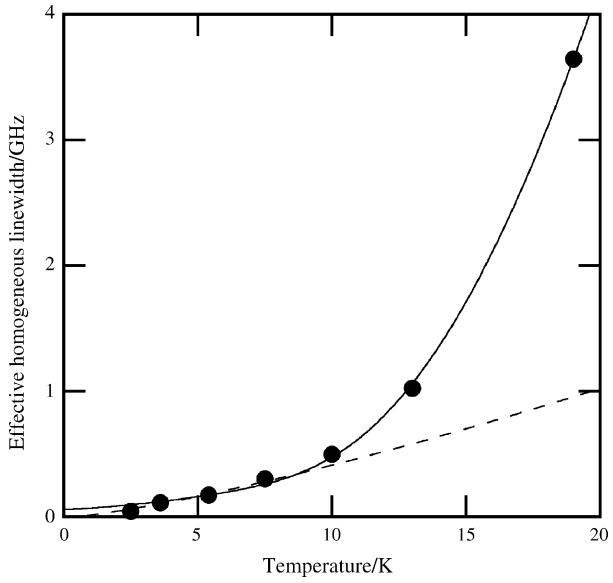

Fig. 18. Temperature dependence of the effective homogeneous line width, Γ_{eff}, of the R_1-line of $[Cr(NCS)_6]^{3-}$/glycerol. The solid line is a fit to Eq. (5); the dashed line is the $T^{1.3}$ power law.

3.2. Hole-burning in ^{3}LC transitions

Spectral hole-burning was conducted on the triplet ligand-centred transition, ^{3}LC, transition of $[Rh(phpy)(bpy)_2]^+$ [54] and $[IrCl_2(5,6\text{-methyl-phen})_2]^+$ [55] by tuning the 457.9 and 488.0 nm lines of an Ar^+ laser, respectively, by changing the temperature of an intracavity etalon. Relatively broad holes were observed. The limited hole width must be due to spectral diffusion because the singlet ground state cannot be subject to electron-spin–electron-spin or electron-spin–nuclear-spin interactions.

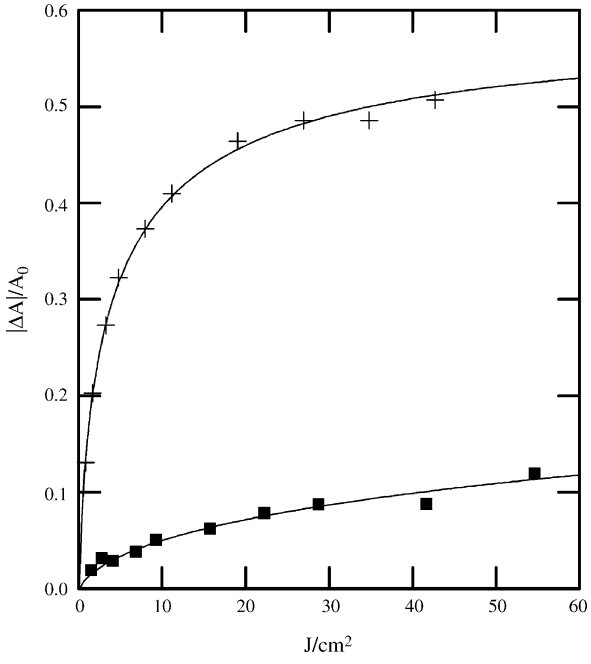

Fig. 19. Effect of host deuteration at 3 K on the hole-burning efficiency of $[Cr(oxalate)_3]^{3-}$ in ethylene:water (2:1, v/v). Crosses and solid squares show the data in the perprotonated and perdeuterated samples, respectively. The solid lines are best fits to Eq. (19).

Also, some magnetic field dependence was observed for the $[Rh(phpy)(bpy)_2]^+$/glycerol system. More work is needed to establish the potential of hole-burning spectroscopy in this class of compounds.

4. Spectral hole-burning of coordination complexes in crystalline systems

4.1. Applications to ^{3}MLCT transitions

The lowest-excited ^{3}MLCT states of ruthenium(II) and osmium(II) diimine complexes in crystalline hosts were extensively studied by a wide range of experiments [56–62]. In particular, the $[Ru(bpy)_3]^{2+}$ and $[Os(bpy)_3]^{2+}$ complexes were investigated as the neat perchlorate and hexafluorophosphate salts and in the $[Zn(bpy)_3](ClO_4)_2$ and $[Ru(bpy)_3](PF_6)_2$ hosts, respectively [56,57]. Racemic $[Zn(bpy)_3](ClO_4)_2$ and $[Ru(bpy)_3](ClO_4)_2$ are isomorphous and crystallize in the monoclinic space group $C2/c$ with four formula units per unit cell [63]. All cations are equivalent but within a single cation one ligand lies about the symmetry axis (crystal b axis) while the other two ligands are crystallographically equivalent, being related by the symmetry axis. Thus, as follows a priori from the crystal structure, the ^{3}MLCT transition cannot involve all ligands to the same degree. From a simple point charge calculation the ^{3}MLCT transition to the crystallographically unique bpy ligand is estimated to be about 900 cm^{-1} above the transitions to the two equivalent ligands. This energy difference manifests itself in polarized absorption spectra in the ^{1}MLCT region.

Racemic $[Ru(bpy)_3](PF_6)_2$ crystallizes in the trigonal space group $P\bar{3}c1$ at room temperature with a phase change to the trigonal space group $P31c$ at 190 K [64]. Thus in this structure the ligands are crystallographically equivalent.

Selective deuteration experiments were particularly successful in demonstrating the localized nature of the lowest three electronic origins in $[Ru(bpy)_3](PF_6)_2$ and $[Ru(bpy)_3]^{2+}$/$[Zn(bpy)_3](ClO_4)_2$. For example, in $[Ru(bpy)_{3-x}(bpy\text{-}d_n)_x]^{2+}$ complexes (with $n = 2$, 6, 8 and $x = 1$ or 2), distinct transitions to the bpy and the bpy-d_n ligand, with the correct intensity ratios, are observed [65]. Another research group has invoked a multiple-site hypothesis to account for the observation of the two sets of electronic origins [66]. However, this hypothesis could be refuted by transient spectral hole-burning experiments as is illustrated in Fig. 20 [57].

In Fig. 20 a transient hole-burning spectrum of $[Ru(bpy)(bpy\text{-}d_8)_2]^{2+}$/$[Zn(bpy)_3](ClO_4)_2$ is shown. Upon burning a spectral hole into the electronic origin II-h_8 of the bpy-h_8 ligand, side holes can be observed at higher energy in the transitions II-d_8 and III-d_8 of the bpy-d_8 ligand. This unequivocally demonstrates that the two sets of transitions occur on one single cation and are not due to two sites.

This example also demonstrates that moderate resolutions on the order of magnitude of 1 cm^{-1} are often sufficient to solve chemical problems.

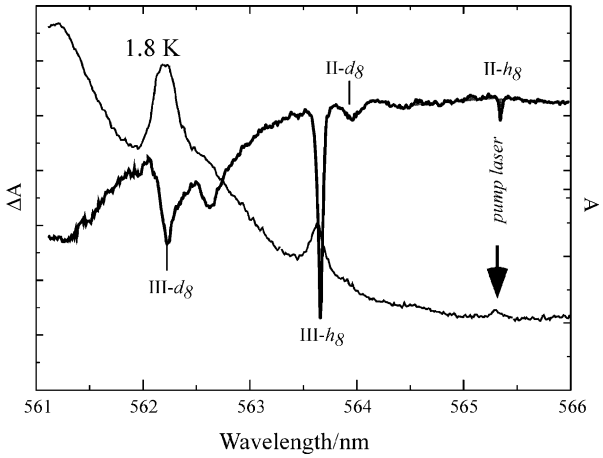

Fig. 20. Transient spectral hole-burning in $[Ru(bpy\text{-}d_8)_2(bpy)]^{2+}/[Zn(bpy)_3](ClO_4)_2$ at 1.8 K. The pump laser is in resonance with the II-h_8 transition. The absorption spectrum is shown for comparison.

4.2. Exchange interactions facilitate narrow spectral holes in concentrated materials

In systems with paramagnetic centers the observed hole widths grow rapidly with increasing concentration, and in order to approach the homogeneous line width extremely low concentrations (≤0.001%) have to be used. The dependence of the hole width on the concentration is mostly due to the fact that electron-spin–electron-spin interactions are governing the effective width at low temperatures, certainly at often used dopant concentrations of about 0.5%. Exchange interactions provide a tool to minimize these interactions since the lowest ground state level has a total spin of $S=0$ in anti-ferromagnetically coupled dimers.

For example, binuclear chromium(III) complexes are usually subject to anti-ferromagnetic coupling, resulting in an $S=0$ lowest $^4A_2{}^4A_2$ ground state level [67]. Electron-spin–electron-spin interactions cannot occur in the $S=0$ ground state. Consequently, dephasing due to these interactions is eliminated for the transition involving the $S=0$ ground state level as long as the number of chromophores in the $^2E^4A_2$ excited state is kept minimal. Thus, electronic origins from the $S=0$ level are only subject to dephasing in the excited state caused by nuclear spin fluctuations and by energy transfer processes that are relatively slow due to the low transition dipole strengths involved. The anti-ferromagnetic coupling in binuclear chromium(III) complexes is well described by following Heisenberg–Dirac–VanVleck operator:

$$H = -2J\vec{S}_1 \cdot \vec{S}_2 - j(\vec{S}_1 \cdot \vec{S}_2)^2 + D_s[S_z^2 - \tfrac{1}{3}S(S+1)] \qquad (24)$$

The first term in Eq. (24) describes the bilinear exchange interaction, the second term accounts for biquadratic exchange and magnetostriction, and the third term is an axial anisotropy term, accounting for the zero-field splitting of the levels with total spin S. If J is negative and large, only the $S=0$ level is populated at liquid helium temperatures, preventing fast dephasing by electron-spin–electron-spin interactions as is discussed above. Surprisingly, with the exception of some work by the author of the present review [68] (see below), it appears that this specific property has not been taken advantage of. Moreover, spectral hole-burning work in excitations of binuclear transition metal or rare earth complexes has received very little attention in general [69].

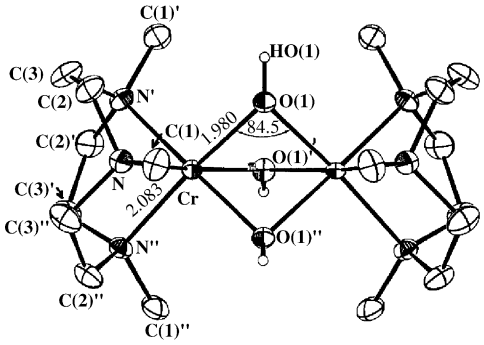

Fig. 21. The trigonal structure of the binuclear complex $[LCr(III)(\mu\text{-}OH)_3Cr(III)L]^{3+}$ (L = 1,4,7-trimethyl-1,4,7-triazacyclononane). The point symmetry of this cation is C_{3h}.

From extensive studies of conventional luminescence, absorption and Zeeman spectra of $[LCr(III)(\mu\text{-}OH)_3Cr(III)L](ClO_4)_3\cdot H_2O$ (L = 1,4,7-trimethyl-1,4,7-triazacyclononane) [70], it followed that the levels of the $^4A_2{}^4A_2$ ground state are well described by Eq. (24) with the parameters $J=64\pm0.3$, $j=1.6\pm0.5\,cm^{-1}$, and $D_1=2.25\pm0.1\,cm^{-1}$. Fig. 21 illustrates the structure of this remarkable binuclear complex.

The strength of the exchange interaction in this trigonal complex (C_{3h} point symmetry) is based on the very short Cr^{3+}–Cr^{3+} distance of 2.66 Å and an analysis of the excited state levels indicated the dominance of the exchange interaction of the $t_{2\chi0}$ orbitals. Due to the large splitting between the $S=0$ and $S=1$ levels of the ground state, only the $S=0$ level is populated at liquid helium temperatures.

We have reported some properties of non-photochemical spectral holes for the $^2E^4A_2 \leftarrow {}^4A_2{}^4A_2$ transitions in single crystals of perprotonated and partially deuterated (lattice water and hydroxo bridges) binuclear $[LCr(III)(\mu\text{-}OH)_3Cr(III)L](ClO_4)_3\cdot H_2O$ (L = 1,4,7-trimethyl-1,4,7-triazacyclononane) [68]. Indeed, relatively narrow holes of $\Gamma\approx80$ MHz were observed, confirming the above discussed ideas: anti-ferromagnetic coupling facilitates narrow spectral holes in *undiluted* Cr^{3+} compounds. The upper limit for the "effective" homogeneous line width of ca. 40 MHz is likely limited by fast excitation energy transfer processes in the concentrated material.

Fig. 22 shows a spectral hole burnt into the $^3E'' \leftarrow {}^1A_1'$ transition of perprotonated $[LCr(III)(\mu\text{-}OH)_3Cr(III)L](ClO_4)_3\cdot H_2O$ at 685.1 nm in α polarization. The inhomogeneous width, Γ_{inh}, of this transition is ca. $0.5\,cm^{-1}$. Very high initial hole-burning efficiencies of 1% and 4% were estimated for the partially deuterated and perprotonated system, respectively, at 2.5 K, using Eq. (20). Spontaneous hole-filling occurs on the minute and hour timescale for the perprotonated and partially deuterated samples, respectively, at 2.5 K, but the rates increase dramaticaly at ca. 7 K. The hole-burning work also indicated that previous spinor assignments were incomplete.

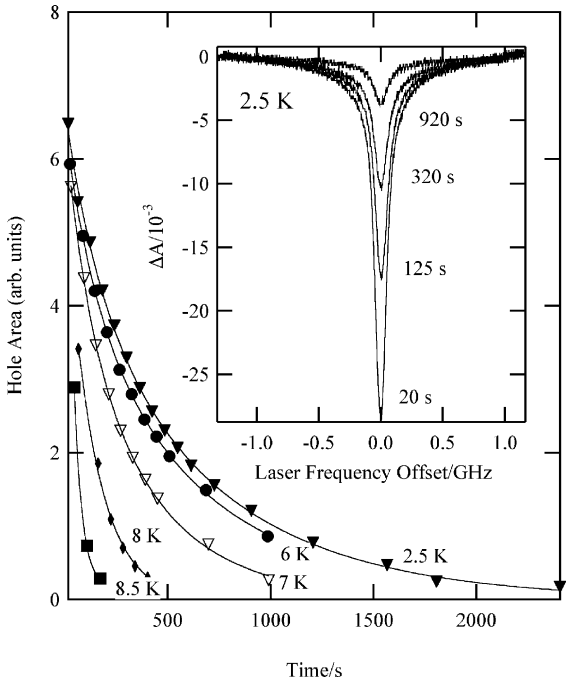

Fig. 22. Spontaneous hole-filling of spectral holes burnt in α polarization into the $^3E'' \leftarrow {}^1A_1'$ transition at 685.1 nm in perprotonated [LCr(III)(μ-OH)$_3$Cr(III)L](ClO$_4$)$_3$·H$_2$O (L = 1,4,7-trimethyl-1,4,7-triazacyclononane). The holes were burnt at 2.5 K for 4 min and the temperature was rapidly ramped to the measurement temperature for $T > 2.5$ K. The fit curves are bi-exponentials for the 2.5, 6 and 7 K measurements. A single exponential was used for the 8 and 8.5 K data. The inset shows the spectral hole for four waiting times at 2.5 K [68].

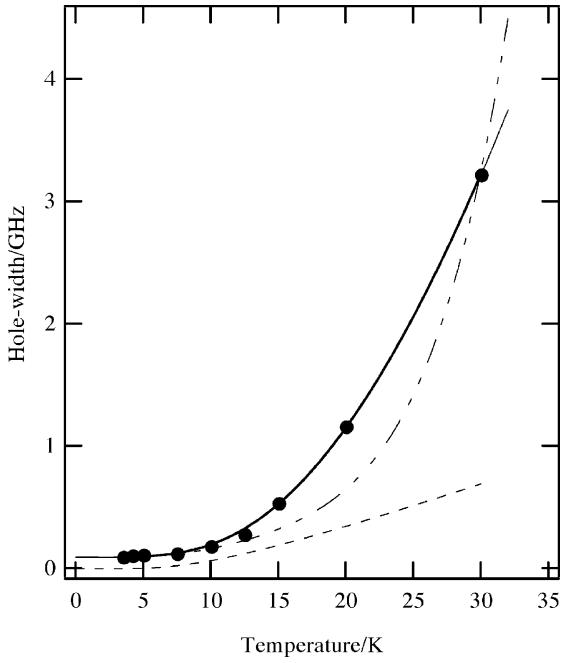

Fig. 23. Temperature dependence of the R_1-line of NaMgAl(oxalate)$_3$·9H$_2$O:Cr(III). The dashed line shows the contribution by the direct process. The dash-dotted line is a fit using the T^7 power law. The solid line uses a local two-vibration Raman model [71].

The fact that anti-ferromagnetic coupling can facilitate narrow spectral holes in undiluted materials points to the potential of coordination chemistry in the design of "ideal" hole-burning materials.

4.3. Temperature dependence of the homogenous line width in crystalline systems

We have recently investigated the temperature dependence of the effective homogeneous line width of the R_1-line in NaMgAl(oxalate)$_3$·9H$_2$O:Cr(III) by transient hole-burning spectroscopy [71]. At low temperature the 90 MHz hole width ($=2\Gamma_{hom}$) is limited by electron-spin–electron-spin interactions because a very high chromium(III) concentration of 4% was employed. In later work zero field hole widths of 40 and 19 MHz were found for samples containing 1.0% [72] and 0.5% chromium(III) [73], respectively. The observed hole width for the R_2-line of 1.1 GHz directly determines the $R_2 \rightarrow R_1$ relaxation rate, and hence the contribution to the R_1-line width can be calculated as a function of temperature using Eq. (6). At temperatures above 10 K the two-phonon Raman process by two local modes becomes the dominant contribution to the line width [71] (see Fig. 23).

The first investigation of the temperature dependence of the homogeneous line width of an electronic origin in a coordination compound was conducted by employing the fluorescence line narrowing technique to the R_1-line of $[Cr(bpy)_3]^{3+}$ embedded in $[Rh(bpy)_3](PF_6)_3$ [74] (not illustrated here). In this early study the observed line width at low temperature was also limited by the relatively high chromium(III) concentration of 0.5% leading to significant electron-spin–electron-spin interactions. The temperature dependence was studied in the range of 1.5–200 K. Again, the direct process between the ^2E levels and two-phonon Raman processes were found to account for the temperature dependence. The latter was calculated by using Eq. (8) and an effective density of phonon states as approximated from the vibrational sidelines in the luminescence spectrum.

4.4. Magnetic field effects in spectral hole-burning

We have demonstrated that the high resolution provided by spectral hole-burning measurements facilitates the determination of g-factors in the excited state and the ground state by the application of low (<10 mT) external magnetic fields [72,73]. An example of this work is illustrated in Fig. 24 where a transient hole-burning experiment in the $R_1(\pm 1/2)$-line was conducted in a magnetic field of $B \| c = 15.3$ mT in NaMgAl(oxalate)$_3$·9H$_2$O:Cr(III). The resulting hole pattern exhibits side holes at the ground state splitting, the excited state splitting and the sum and difference of the ground and excited state splittings. Hence, the g-factor is determined both in the ground state and the excited state to high accuracy.

Upon the application of an external magnetic field a significant narrowing of the resonant hole width is observed. For example, the resonant hole displays a width of 4 and <1 MHz in magnetic fields $B \| c$ of 7.3 and 15.3 mT, respectively. This magnetic field induced narrowing implies that electron-spin–electron-spin

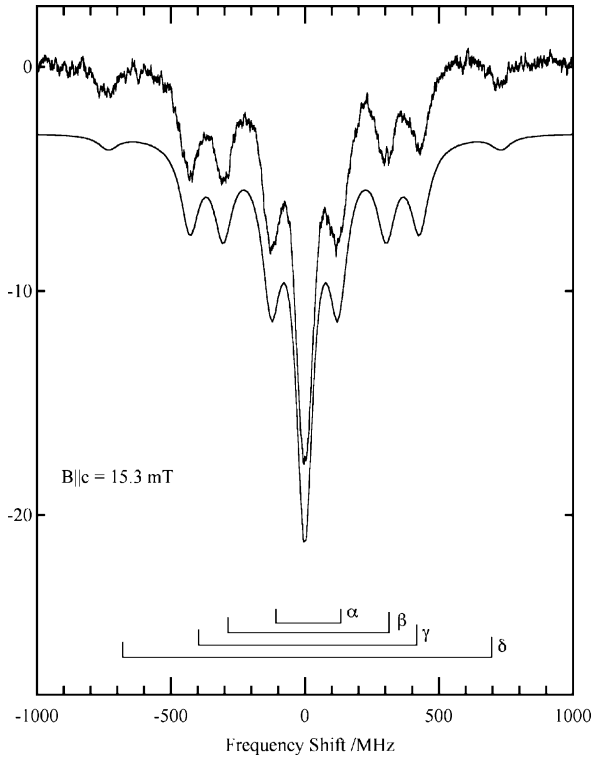

Fig. 24. Transient spectral hole-burning in the $R_1(\pm 1/2)$-line of NaMgAl(oxalate)$_3$·9H$_2$O:Cr(III) in $B\|c = 15.3$ mT and 2.5 K. The smooth line is the result of a simulation. α, β, γ and δ indicate twice the difference of excited and ground state splittings, the excited state splitting, the ground state splitting and the sum of the excited and ground state splittings, respectively [73].

interactions are the main dephasing mechanism at 2.5 K in 0.5–1% samples.

We have also conducted magnetic field experiments in *persistent* spectral hole-burning of the R_1-line in NaMgAl(oxalate)$_3$·9H$_2$O:Cr(III) [75]. The most interesting aspect of this work is the fact that the *same* hole pattern results in a magnetic field after burning in zero field, and in zero field after burning in the same field. The latter thus provides a persistent memory of magnetic fields. This is illustrated in Fig. 25 where the two lower traces in panels (a) and (b) are identical.

Possible applications include the temporal profiling of pulsed magnets, magnetic fluctuations in laboratories or, for example, in the vicinity of astronomical objects as probed on spacecrafts.

The magnetic field effects with $B\|c$, both in persistent and transient spectral hole-burning, can be interpreted by using the schematic energy level diagram shown in Fig. 26.

4.5. Extraordinary deuteration effect

Upon partial deuteration of NaMgAl(oxalate)$_3$·9H$_2$O:Cr(III) a 1000-fold *increase* in the hole-burning efficiency in the R_1-line has been observed [53] (Fig. 27). This was an unexpected result because usually the hole-burning efficiency decreases upon deuteration (see Section 3.1). It is well established that water molecules of crystallization can flip by 180° in crystalline solids, including oxalates [76–78]. The enormous increase in the hole-burning efficiency in the partially deuterated sample can thus be rationalized by a mechanism that is based on water flips. After the flip, the zero point energies in the ground state and the excited state change by different amounts, leading to slight shifts in the transition frequency. This is because the hydrogen isotope (^{1}H, ^{2}H), that undergoes hydrogen bonding with the oxygen atom of the oxalate ligand, is exchanged by the flip. Hence, upon each photoinduced flip a chromophore's transition frequency is shifted out of resonance with the laser and the "photoproducts" yield sharp anti-holes.

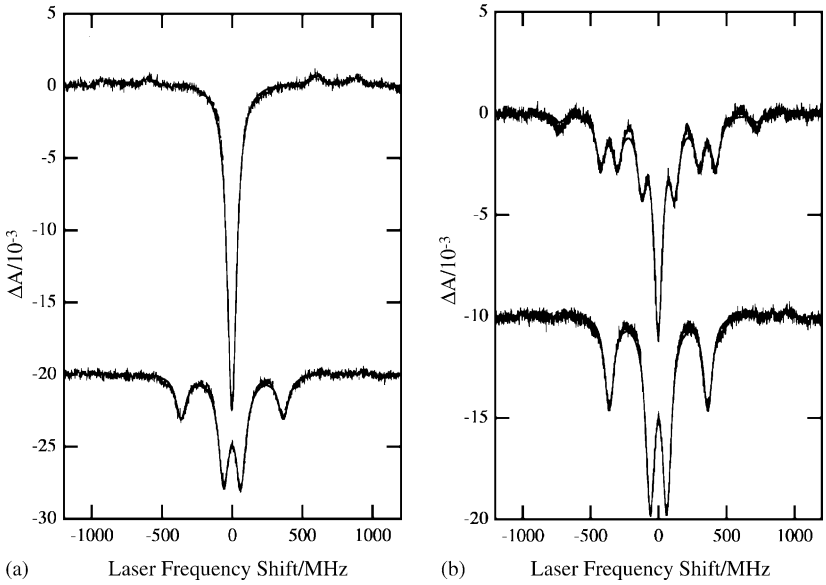

Fig. 25. Memory effect in persistent spectral hole-burning in the $R_1(\pm 1/2)$-line of 50% deuterated NaMgAl(oxalate)$_3$·9H$_2$O:Cr(III) at 2.5 K. In (a) the hole was burnt in zero field (upper trace) and then a magnetic field $B\|c = 15.3$ mT was applied (lower trace). In (b) the hole was burnt in $B\|c = 15.3$ mT (upper trace) and then the field was switched off (lower trace) [75].

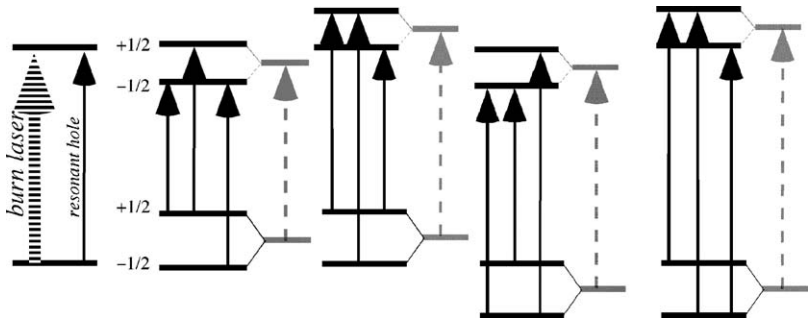

Fig. 26. Schematic energy level diagram for the magnetic field effects with $B\|c$ in transient and persistent spectral hole-burning of the $R_1(\pm1/2)$-line in $NaMgAl(oxalate)_3{\cdot}9H_2O$:Cr(III). The dark bars show the levels in the field leading to the hole pattern of Fig. 24 and upper trace of Fig. 25b. The grey bars indicate the levels after the field has been switched off in persistent spectral hole-burning (lower trace of Fig. 25b).

4.6. Measuring spin-lattice relaxation times in the excited state and the ground state

If very low concentrations of a paramagnetic impurity are used it becomes possible to measure spin-lattice relaxation times both in the excited state and the ground state by time-resolved transient spectral hole-burning experiments. (At higher concentrations cross-relaxation effects lead to fast relaxation rates of the chromophores that are resonant with the laser.) We have demonstrated this effect in transient spectral hole-burning in the R_1-line in very low chrome (0.0017% per weight) emerald, $Be_3Al_2Si_6O_{18}$:Cr(III) [79]. Although this is not a coordination compound per se, it can be used as a model system.

The experiment illustrated in Fig. 28 was conducted on the $R_1(\pm3/2)$-line. In an external magnetic field $B\|c$ the $\pm3/2$ levels in the ground state (gs) and the $\pm1/2$ spin levels of the $2\bar{A}$ (^2E) excited state (ex) split by $3g\|(gs)\mu_B B\|c$ and $g\|(ex)\mu_B B\|c$, respectively. If no relaxation occurs between the two levels in the excited state ($\pm1/2$) and the ground state, no side-holes will be observed. If relaxation occurs in the excited state, side holes will appear at the difference of the excited state splitting and ground state splitting. If the system is then deactivated and spin-lattice relaxation is still slow in the ground state, the side-holes will be converted into anti-holes. These effects have indeed been observed; at lowest temperature no side-holes appear due to the very slow relaxation rate in the excited state. At temperatures above 5 K, side-hole to anti-hole conversion can be observed. The time behavior shows three regimes: in the first ≈100 μs a build-up of the side holes occurs due to spin-lattice relaxation in the excited state; the excited state is then deactivated, leading to a decay of the resonant hole with a conversion of the side holes into anti-holes due to ground state level population storage; finally the decay of the residual resonant hole, which is based on ground state level population storage, and the anti-holes occurs due to spin-lattice relaxation in the ground state. From the temperature dependence it follows that the spin-lattice relaxation rates are dominated by Orbach processes in the experimental temperature range (3–12 K). For example, Fig. 29 displays the temperature dependence of the spin lattice relaxation rate in $B\|c = 12.2$ mT between the +3/2 and −3/2 $^4A_2$ ground state spin levels.

Time-resolved transient spectral hole-burning experiments thus facilitate the simultaneous determination of g-factors and spin-lattice relaxation times for both the excited and the ground state. The inherent stability of diode lasers enables hole-burning experiments of highest quality. Moreover, since the frequency of diode lasers can be rapidly swept, it is readily possible to perform time-resolved transient hole-burning experiments on the microsecond timescale. We note here that for saturated holes

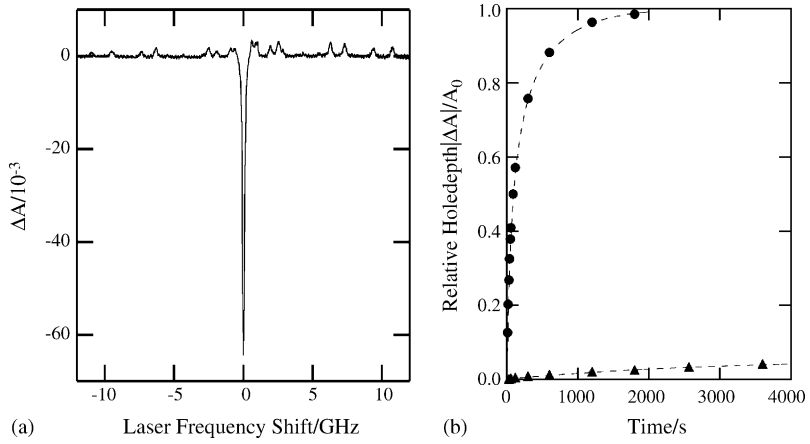

Fig. 27. (a) Spectral hole and anti-holes in 46% deuterated $NaMgAl(oxalate)_3{\cdot}9H_2O$:Cr(III) at 2.5 K. (b) Relative hole depth as a function of the burn time for the same power density for the perprotonated (solid triangles) and partially deuterated sample (solid circles) [53].

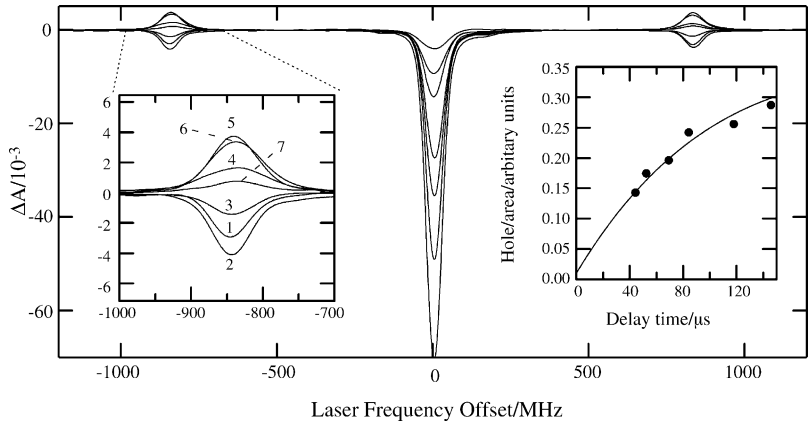

Fig. 28. Time-resolved THB in the $2\bar{A}(^2E) \leftarrow 2\bar{A}$ ($^4A_2$, ±3/2) transition of $Be_3Al_2Si_6O_{18}$:Cr(III) (0.0017%) at 6 K in $B \| c = 12.2$ mT at delay periods of 1, 0.05 ms; 2, 0.324 ms; 3, 0.698 ms; 4, 1.06 ms; 5, 2.62 ms; 6, 4.69 ms and 7, 10.38 ms. The left insert shows the time evolution of the side-hole/anti-hole at −840 MHz. The right insert shows the integrated hole area of the side-hole as a function of short delay periods [79].

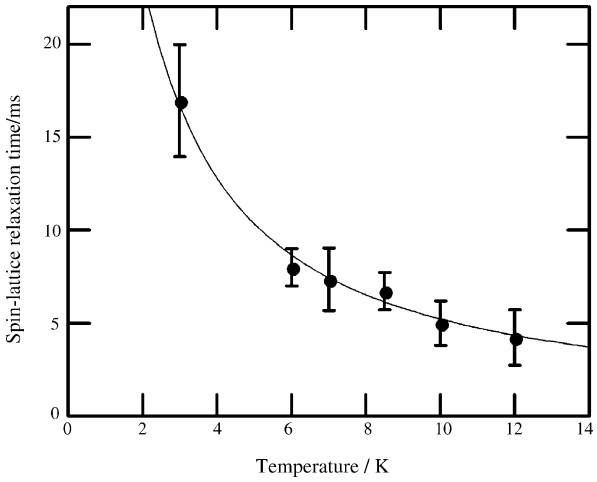

Fig. 29. Temperature dependence of the spin-lattice relaxation time between the +3/2 and −3/2 spin-levels of the $^4A_2$ ground state.

the hyperfine structure associated with ^{53}Cr(III) becomes also visible.

5. Summary and outlook

The present review aims to demonstrate that spectral hole-burning is a highly valuable tool in the elucidation of fine details of the electronic structure of coordination compounds. This laser-based technique allows to overcome the inhomogeneous broadening of electronic transitions, and magnetic properties, spin-lattice relaxation rates, host and guest dynamics, non-photochemical and photochemical hole-burning kinetics, etc. can be probed to greatest accuracy. For example, it is possible to simultaneously measure *g*-factors and spin-lattice relaxation rates in the ground and excited states in minute magnetic fields, greatly simplifying the experimental requirements. We have established that (inexpensive) diode lasers are particularly useful in hole-burning spectroscopy of coordination compounds; they enable fast and reliable transient spectral hole-burning experiments that otherwise need very expensive ion laser/dye laser systems. So far, the spectroscopy has been somewhat restricted by the limited wavelength availability of single longitudinal mode diode lasers and the relatively narrow range (ca. 30 GHz) of mode-hop free tuning. However, as more wavelengths become available for vertical cavity surface emitting laser (VCSEL) diodes, diode laser-based spectroscopy will undertake a quantum leap in terms of significance and importance. This stems from the fact that VCESLs are tunable over a much wider frequency (wavelength) range without mode hops in comparison with Fabry-Perot or DFB diode lasers.

Acknowledgement

I thank Dr. L. Wallace for her help with this manuscript.

References

[1] A. Szabo, Phys. Rev. B 11 (1975) 4512.
[2] B.M. Kharlamov, R.I. Personov, L.A. Bykovskaya, Opt. Commun. 12 (1974) 216.
[3] A.A. Gorokhovskii, R.K. Kaarli, L.A. Rebane, JETP Lett. 20 (1974) 216.
[4] B.H. Soffer, B.B. McFarland, Appl. Phys. Lett. 8 (1966) 166.
[5] M.L. Spaeth, W.R. Sooy, J. Chem. Phys. 48 (1968) 2315.
[6] S.L. Hager, J.E. Willard, J. Chem. Phys. 61 (1974) 3244.
[7] R.M. Macfarlane, R.M. Shelby, in: A.A. Kaplyanskii, R.M. Macfarlane (Eds.), Spectroscopy of Solids Containing Rare Earth Ions, Elsevier, Amsterdam, 1987, p. 51.
[8] W.E. Moerner (Ed.), Persistent Spectral Hole-burning: Science and Applications, Topics in Current Physics, vol. 44, Springer-Verlag, Berlin, 1988.
[9] S. Völker, Annu. Rev. Phys. Chem. 40 (1989) 499.
[10] J. Friedrich, D. Haarer, Angew. Chem. Int. Ed. Engl. 23 (1984) 113.
[11] U.P. Wild, U.P. Wild, A. Rebane, A. Renn, Adv. Mater. 3 (9) (1991) 453.
[12] S.A. Basun, M. Raukas, U. Happek, A.A. Kaplyanskii, J.C. Vial, J. Rennie, W.M. Yen, R.S. Meltzer, Phys. Rev. B 56 (1997) 12992.
[13] M.J. Sellars, R.S. Meltzer, P.T.H. Fisk, N.B. Manson, J. Opt. Soc. Am. B 11 (1994) 1468.
[14] (a) S. Fei, H.L. Strauss, J. Phys. Chem. 100 (1996) 3414;
(b) S.T. Robertson, H.L. Strauss, J. Phys. Chem. A 107 (2003) 4226;
(c) Y.-H. Cha, H.L. Strauss, J. Phys. Chem. A 104 (2000) 8617;
(d) H.L. Strauss, Acc. Chem. Res. 30 (1997) 37.

[15] (a) H. Riesen, Struct. Bond. 107 (2004) 179;
(b) E. Krausz, H. Riesen, in: E. Solomon, A.B.P. Lever (Eds.), Laser Spectroscopy in Inorganic Electronic Structure and Spectroscopy, vol. I, Wiley, New York, 1999, p. 307.
[16] N. Bloembergen, Physica (Utrecht) 25 (1949) 386.
[17] (a) J. Ganem, Y.P. Wang, D. Boye, R.S. Meltzer, W.M. Yen, R.M. Macfarlane, Phys. Rev. Lett. 66 (1991) 695;
(b) J. Ganem, Y.P. Wang, D. Boye, R.S. Meltzer, W.M. Yen, R. Wannemacher, R.M. Macfarlane, Phys. Rev. Lett. 66 (1991) 1649.
[18] R.M. Shelby, C.S. Yannoni, R.M. Macfarlane, Phys. Rev. Lett. 41 (1978) 1739.
[19] R.G. DeVoe, A. Wokaun, S.C. Raun, R.G. Brewer, Phys. Rev. B 23 (1981) 3125.
[20] A. Szabo, Opt. Lett. 8 (1983) 486.
[21] G.F. Imbusch, W.M. Yen, A.L. Schawlow, D.E. McCumber, M.D. Sturge, Phys. Rev. 133 (1964) A1029.
[22] D.E. McCumber, M.D. Sturge, J. Appl. Phys. 34 (1963) 1682.
[23] B. Di Bartolo, R. Peccei, Phys. Rev. 137 (1965) A1770.
[24] A. Freiberg, L.A. Rebane, Phys. Stat. Sol. B: Basic Res. 81 (1977) 59.
[25] M. Glasbeek, D.D. Smith, J.W. Perry, W.R. Lambert, A.H. Zewail, J. Chem. Phys. 79 (1963) 2145.
[26] D.D. Hsu, J.L. Skinner, J. Chem. Phys. 83 (1985) 2107.
[27] R. Jankowiak, J.M. Hayes, G.J. Small, Chem. Rev. 93 (1993) 1471.
[28] P.W. Anderson, B.I. Halperin, C.M. Varma, Phil. Mag. 25 (1972) 1.
[29] W. Köhler, J. Friedrich, Phys. Rev. Lett. 59 (1987) 2199.
[30] S. Völker, R.M. Macfarlane, A.Z. Genack, H.P. Trommsdorf, J.H. Van der Waals, J. Chem. Phys. 67 (1977) 1759.
[31] M.A. Drobizhev, M.N. Sapozhnikov, Chem. Phys. Lett. 236 (1995) 438.
[32] A.V. Turukhin, A.A. Gorokhovsky, Chem. Phys. Lett. 317 (2000) 109.
[33] R. Jankowiak, R. Richert, H. Bässler, J. Phys. Chem. 89 (1985) 4569.
[34] (a) Y. Bai, M.D. Fayer, J. Chem. Phys. 128 (1990) 135;
(b) K.A. Littau, Y.S. Bai, M.D. Fayer, Chem. Phys. Lett. 159 (1989) 1.
[35] P.N. Schatz, S. Piepho, Group Theory and Spectroscopy, Wiley, New York, 1983.
[36] N.M. Strickland, R.L. Cone, R.M. Macfarlane, Phys. Rev. B 59 (1999) 14328.
[37] G.J. Pryde, T. Bottger, R.L. Cone, R.C.C. Ward, J. Lumin. 98 (2002) 309.
[38] C.W. Thiel, Y. Sun, R.L. Cone, J. Mod. Opt. 49 (2002) 2399.
[39] H. Sónajalg, A. Gorokhovskii, R. Kaarli, V. Palm, M. Rätsep, P. Saari, Opt. Commun. 71 (1989) 377.
[40] V. Lavielle, F. De Seze, I. Lorgeré, J.-L. Le Gouët, J. Lumin. 107 (2004) 75.
[41] M.S. Shahriar, P.R. Hemmer, S. Lloyd, P.S. Bhatia, A.E. Craig, Phys. Rev. A 66 (2002) 032301.
[42] G. Casto, D. Haarer, R.M. Macfarlane, H.P. Trommsdorff, Frequency selective optical data storage system, US Patent No. 4,101,976 (1978).
[43] W.R. Babbitt, Y.S. Bai, T.W. Mossberg, Proc. Soc. Photo-Opt. Instrum. Eng. 639 (1986) 240.
[44] R. Ao, L. Kümmerl, D. Haarer, Adv. Mater. 7 (1995) 495.
[45] H. Riesen, N.B. Manson, Chem. Phys. Lett. 161 (1989) 131.
[46] H. Riesen, E. Krausz, J. Chem. Phys. 97 (1992) 7902.
[47] H. Riesen, E. Krausz, L. Dubicki, Chem. Phys. Lett. 218 (1994) 579.
[48] M. Lewis, H. Riesen, Phys. Chem. Chem. Phys. 4 (2002) 4845.
[49] H. Riesen, J. Phys. Chem. A 104 (2000) 5469.
[50] T.M.H. Creemers, J.M.A. Koedijk, I.Y. Chan, R.J. Silbey, S. Völker, J. Chem. Phys. 107 (1999) 4797.
[51] T. Monks-Corrigan, H. Riesen, Chem. Phys. Lett. 419 (2006) 321.
[52] W. Breinl, J. Friedrich, D. Haarer, J. Chem. Phys. 81 (1984) 3915.
[53] H. Riesen, J. Hughes, Chem. Phys. Lett. 372 (2003) 563.
[54] H. Riesen, E. Krausz, A. Zilian, H.U. Güdel, Chem. Phys. Lett. 182 (1991) 271.
[55] H. Riesen, E. Krausz, L. Wallace, J. Phys. Chem. 96 (1992) 3621.
[56] H. Riesen, L. Wallace, E. Krausz, Int. Rev. Phys. Chem. 16 (1997) 291.
[57] H. Riesen, L. Wallace, E. Krausz, Inorg. Chem. 39 (2000) 5044.
[58] R.W. Harrigan, G.A. Crosby, J. Chem Phys. 59 (1973) 3468-76.
[59] P.G. Bradley, N. Kress, B.A. Hornberger, R.F. Dallinger, W.H. Woodruff, J. Am. Chem. Soc. 103 (1981) 7441.
[60] K. Kalyanasundaram, Coord. Chem. Rev. 46 (1982) 159.
[61] A. Juris, V. Balzani, F. Barigelletti, S. Campagna, P. Belser, A. von Zelewsky, Coord. Chem. Rev. 84 (1988) 95.
[62] E. Krausz, J. Ferguson, Prog. Inorg. Chem. 37 (1989) 293.
[63] E. Krausz, H. Riesen, A.D. Rae, Aust. J. Chem. 48 (1995) 929.
[64] M. Biner, H.-B. Bürgi, A. Ludi, C. Röhr, J. Am. Chem. Soc. 114 (1992) 5197.
[65] H. Riesen, L. Wallace, E. Krausz, J. Phys. Chem. 100 (43) (1996) 17138.
[66] P. Huber, H. Yersin, J. Phys. Chem. 97 (1993) 12705.
[67] P.J. McCarthy, H.U. Güdel, Coord. Chem. Rev. 88 (1988) 69.
[68] H. Riesen, Chem. Phys. Lett. 383 (2004) 512.
[69] F. Ramaz, J.C. Vial, R.M. Macfarlane, J. Lumin. 53 (1992) 244.
[70] H. Riesen, H.U. Güdel, Mol. Phys. 60 (1987) 1221.
[71] M. Lewis, H. Riesen, J. Phys. Chem. 106 (2002) 8039.
[72] J. Hughes, H. Riesen, Chem. Commun. (2002) 1616.
[73] J. Hughes, H. Riesen, J. Phys. Chem. A 107 (2003) 35.
[74] H. Riesen, J. Lumin. 54 (1992) 71.
[75] H. Riesen, J. Hughes, Chem. Phys. Lett. 370 (2003) 26.
[76] K. Larsson, J. Tegenfeldt, J. Mol. Struct. 178 (1988) 315.
[77] C. Nöldeke, B. Asmussen, W. Press, H. Büttner, G. Kearle, Chem. Phys. 289 (2003) 275.
[78] B. Pedersen, W.G. Clark, J. Chem. Phys. 53 (1970) 1024.
[79] B. Hayward, H. Riesen, Phys. Chem. Chem. Phys. 7 (2005) 2579.